RSC Advances

PAPER

View Article Online
View Journal | View Issue

Cite this: *RSC Adv.*, 2021, **11**, 847

Slippery liquid infused porous surfaces with corrosion resistance potential on aluminum alloy

Peng Yu, Zhongxu Lian, Jinkai Xu* and Huadong Yu*

The slippery liquid infused porous surface has developed into a potential technology to solve the problem of poor durability in corrosion resistance. Herein, a kind of slippery liquid infused porous surface is created on 7075 aluminum alloy by wire electrical discharge machining for corrosion resistant applications. The hardness of the constructed porous microstructure is similar to the aluminum alloy substrate material, which ensures the stability of the slippery liquid infused porous surface. The modification of low surface energy substance fluorosilane avoids the direct contact between corrosive liquid and porous surface, and improves the lyophobic performance of the porous microstructure surface. The corrosion resistance of the porous microstructure surface is enhanced by the injection of perfluorinated lubricating oil. The experimental results show that the created slippery liquid infused porous surface can display super-slippery properties and durable corrosion resistance. The average sliding velocity of a water droplet is 0.48 ± 0.05 mm s^{-1} at a sliding angle of 5°. The corrosion current density of the surface is 3.116×10^{-6} A cm^{-2}, which is 2 orders of magnitude lower than that of the polished surface. And the impedance radius reaches 90 kΩ cm^2, which is about 20 times that of the polished surface.

Received 12th October 2020
Accepted 7th December 2020

DOI: 10.1039/d0ra08674f

rsc.li/rsc-advances

1. Introduction

The high-strength aluminum alloy, including the 2XXX, 6XXX, and 7XXX series, is one of the most widely used non-ferrous metal materials in industry.[1] Because of its good mechanical and physical properties, it is widely used in the fields of aviation, aerospace, automobiles and mechanical manufacturing.[2–4] However, due to its active chemical properties and poor corrosion resistance in harsh environments, the application of aluminum alloys in corresponding fields is restricted.[5,6] Therefore, it is of great significance to improve the corrosion resistance and prolong the service life of aluminum alloy by surface treatment technology. Corrosion resistance technology mainly includes electrochemical protection,[7] surface nano crystallization protection[8] and preparation of a superhydrophobic surface.[9–12] Slippery liquid infused porous surfaces (SLIPS) use lubricating oil to replace the air in the microstructure gap on the surface of the substrate, with the help of capillary action to lock the lubricating oil in the microstructure and form an oil film on the substrate. The oil film blocks the contact between corrosive liquid and substrate, so as to achieve the purpose of corrosion resistance. In recent years, SLIPS has gradually become one new technology to replace the above corrosion resistance technologies.[13,14] The fluidity of lubricant provides the SLIPS with an ability to repair itself, which is an advantage of SLIPS similar to superhydrophobic surfaces,[15–17] the SLIPS has broad application prospects in many other fields including anti-icing,[18,19] self-cleaning[20] and bioengineering.[21]

The SLIPS is usually developed based on superhydrophobic substrates and there are many excellent works in the field of superhydrophobic substrates. Dr Song[22] proposed a mold replication technology to realize the large-scale fabrication of superhydrophobic conical pillars with high mechanical strength Boinovich[23] considered the role of different mechanisms of corrosion protection, related to the superhydrophobic state of the surface. The corrosion current density of the superhydrophobic coatings contacted with 3 M solutions of KCl during 2 h can reached 4.0×10^{-11} A cm^{-2}. Up to now, scholars have done a lot of research on the construction of surface porous microstructure required by SLIPS with various methods including chemical reaction,[24] spraying,[25,26] self-assembly,[27,28] electrochemical coating[29] and laser irradiation.[30] For example, Kim[29] reported a direct fabrication method of SLIPS by electrochemical coating and studied the effect of surface structure size and layer distribution on lubricant retention under high shear conditions by comparing the loss of lubricants, contact angle lag and sliding angle of water and ethanol droplets on different surfaces. Yeong[30] prepared a flexible superhydrophobic silica gel material by copying the micro-texture of laser-irradiated aluminum substrate to polydimethylsiloxane, by injecting silicone oil into the microstructures, the material achieved the anti-icing property. Although the preparation of porous microstructure has been made significant progress, the

Ministry of Education Key Laboratory for Cross-Scale Micro and Nano Manufacturing, College of Mechanical and Electric Engineering, Changchun University of Science and Technology, Changchun 130022, China. E-mail: yuhuadong@cust.edu.cn; xujinkai2000@163.com

problems of high cost, low efficiency, poor stability and durability have not been solved. For example, the raw materials used in spraying method are expensive, some of which are organic and harmful to health. The biggest disadvantage of self-assembly technology is that the stability is slightly poor, and the structure is easy to be destroyed under the action of some solvents. The problem of preparing porous structure by chemical reaction is low efficiency.

In this paper, the porous microstructure is constructed on the surface of 7075 aluminum alloy by a novel wire electrical discharge machining (WEDM). The principle of WEDM is to use high temperature melting and vaporizing materials produced by pulse discharge between tool electrode and workpiece electrode, which enables precision machining of porous microstructure on metal surface.[31] Due to the rapid cooling of coolant, a recast layer with porous microstructure is formed on the surface, and its hardness is generally greater than that of the substrate material.[32] This is beneficial to the stability of the porous microstructure required by SLIPS. Furthermore, the processing of planar and various complex shapes of cavity can be achieved by WEDM, it provides conditions for large-area, high-efficiency precision construction of porous microstructure on metal surface. After modification with a low surface energy substance fluorosilane, the prepared porous microstructure surface is injected with perfluorinated lubricating oil to obtain the SLIPS. The corrosion resistance of prepared sample surface treated by different methods is evaluated by potentiodynamic polarization curve measurement, electrochemical impedance spectroscopy test and immersion experiment in 3.5 wt% NaCl solution. The results indicate that the prepared SLIPS provides stable and durable corrosion resistance.

2. Experimental

2.1. Preparation of the SLIPS

Inspired by the super-slippery surface of nepenthes plant, a slippery surface on aluminum alloy substrate (die casting 7075 aluminum alloy plate, a commercial aluminum alloy without overheating treatment) was prepared by liquid injection to realize the stable and durable corrosion resistance property. In this research, the porous microstructure on aluminum alloy substrate was constructed by a multiple cutting method using WEDM technology (Fig. 1). The processing parameters are shown in Table 1. In the electrical machining process, the morphology and size of the porous microstructure are associated with the pulse discharge energy (see Section 3.1 for details). During the first cutting, the surface is roughly processed under a higher discharge energy condition, aiming at quickly removing material. The second and third cuttings are actually a semi-finishing process to correct the size of the workpiece by setting the offset reasonably, and the discharge energy is reduced as compared to that generated during the first cutting process. The fourth cutting is finish machining, the size of the workpiece is corrected again by further reducing the discharge energy, and the surface of the sample is machined to minimize the size of the porous microstructures.

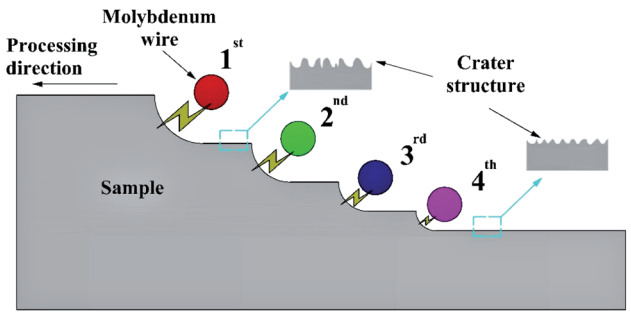

Fig. 1 Schematic diagram of multiple cutting method.

The aluminum alloy samples treated by WEDM were cleaned using ultrasonic vibration with acetone, ethanol and deionized water in turn and dried at room temperature. Then the dry and clean samples were immersed into the modifying solution for 2 hours to reduce surface energy, and taken out for drying. To prepare the modifying solution, fluorosilane and ethanol were mixed at a mass ratio of 1 : 100 and a magnetic mixer was used to mix the content evenly. A micro-injector was used to release 20 μL of perfluorinated lubricating oil (Dupont GPL 103) onto the surface of samples modified by fluorosilane. The angle of inclination of the sample surface was changed continuously to make the lubricating oil spread evenly. Then the sample injected with lubricating oil was inclined at 25° and fixed for 1 hour to ensure that the excessive oil could flow away from the sample surface. The preparation process of the SLIPS is shown as Fig. 2.

2.2. Sample characterization

Scanning electron microscopy (SEM, Zeiss-EVO MA25, Germany) was used to capture the microscopic topography images of the sample surface, and the surface was sprayed with gold and imaged in a low vacuum mode to ensure image quality. Three-dimensional morphology of sample surface was obtained by laser scanning confocal microscope (LSCM, Zeiss-LSM700, Germany). The chemical composition of the sample surface was analyzed by energy dispersive spectrometer (EDS, Oxford-X-Max 20, The United Kingdom) in a plane scanning mode with an area of 50 μm × 50 μm, and the results were average values of 5 different regions. The wettability of the sample surface was measured by developed contact angle measuring instrument using ellipse method (measurement range: 0–180°, reading resolution: 0.01°). The stopwatch was used to record the time and the image was taken by a CCD camera. In order to solve the problem of wettability deviation caused by the uniformity of the surface obtained by the WEDM, the contact angle (CA) was measured repeatedly at five different positions on the surface of the sample.

2.3. Corrosion resistance test

In this paper, the corrosion resistance of aluminum alloy surface treated by different methods was analyzed in detail. A group of polished surface (PS) was taken as experimental control group, and the other three groups were WEDM surface

Table 1 Multiple cutting parameters of WEDM

Cutting order	Wire speed ($m\ s^{-1}$)	Peak current (A)	Pulse width (μs)	Pulse interval (μs)	Peak voltage (V)	Offset (μm)
1st	11.6	19.2	24	96	100	162
2nd	3.9	9.6	6	24	100	102
3rd	3.9	5.12	0.4	6	80	92
4th	3.9	3.2	0.25	2.5	80	90

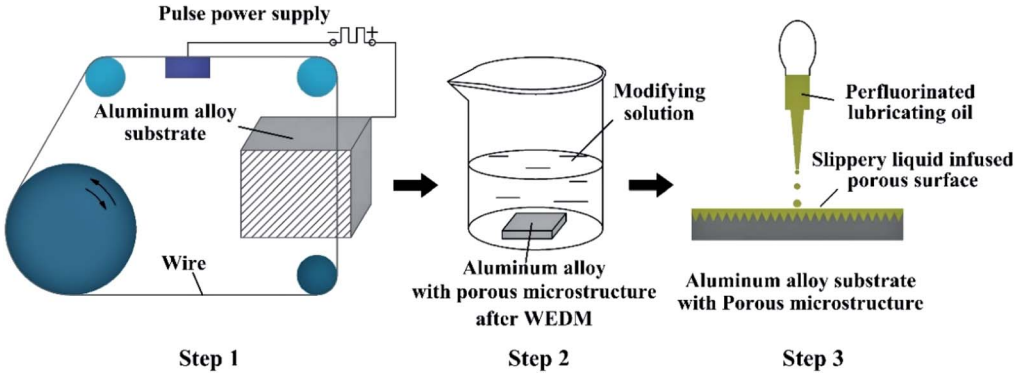

Fig. 2 The preparation process of the SLIPS. Step 1: preparation of rough porous structures on aluminum alloy substrate by WEDM. Step 2: aluminum alloy samples treated by WEDM were immersed into a modifying solution prepared by mixing fluorosilane and ethanol in a ratio of 1 : 100. Step 3: perfluorinated lubricating oil was injected into the porous microstructure on aluminum alloy substrate.

(WEDMS, showing hydrophobicity), WEDM surface modified by fluorosilane (FWEDMS, showing approximate superhydrophobicity) and SLIPS. At room temperature, the corrosion resistance of the sample surface was evaluated by potentiodynamic polarization curve measurement, electrochemical impedance spectroscopy test and immersion experiment in 3.5 wt% NaCl solution. The electrochemical experiments were performed using the Zahner Zennium electrochemical workstation with three-electrode electrolytic cell. The diameter of the circular sheet working electrode was 14 mm and the thickness was 2 mm, the exposed area was 1 cm^2. Platinum electrode and saturated calomel electrode (SCE) were used as counter electrode and reference electrode, respectively. In the potentiodynamic polarization curve measurement, the scanning rate was set to 0.5 mV s^{-1}, and the scanning potential range of each sample was set from −1 V to 1 V (*vs.* open circuit potential). Before the polarization scans started, the electrodes were stabilized for 1 hour in electrolytic cell, and the open circuit potential (OCP) was recorded at the same time (the OCPs of PS, WEDMS FWEDMS and SLIPS were −0.82 mv, −0.72 mv, −0.78 mv, −0.65 mv, respectively). The corrosion potential (E_{corr}) and corrosion current density (I_{corr}) were obtained by Tafel extrapolation method to analyze the corrosion resistance performance of the sample surface. The electrochemical impedance spectroscopy (EIS) were recorded by applying a sinusoidal 10 mV perturbation signal through a frequency domain from 100 kHz down to 10 mHz. The steps per decade of frequency in a single spectrum were set to 4 at lower limit and 8 above 66 Hz. In the salt solution immersion experiment, the samples were immersed in 3.5 wt% NaCl solution. The surface morphology,

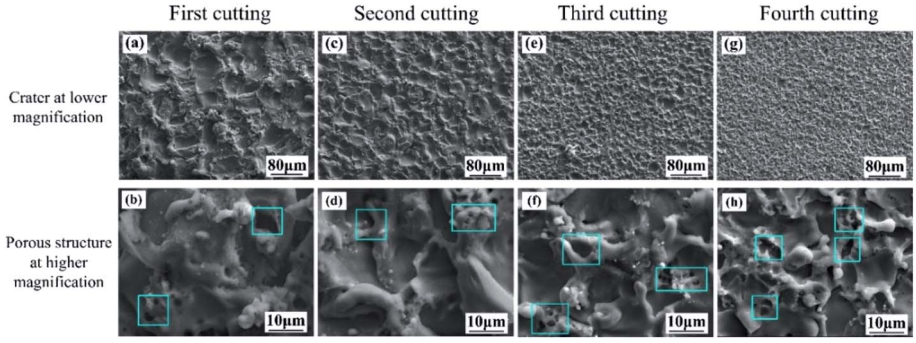

Fig. 3 SEM images of aluminum alloy surface treated by WEDM with different cutting times. (a and b) First cutting. (c and d) Second cutting. (e and f) Third cutting. (g and h) Fourth cutting. (b, d, f and h) are the enlarged views of (a, c, e and g) respectively.

chemical composition and wettability of the samples during immersion were analyzed to evaluate the corrosion resistance.

3. Results and discussion

3.1. Surface micromorphology and wetting performance analysis

Fig. 3 shows the SEM images of aluminum alloy surface treated by WEDM with different cutting times. Fig. 3a and b are the micro morphology of the treated surface after first cutting. It can be seen that many craters with a diameter ranging from 60 to 100 μm were formed on the surface. The craters are surrounded by some porous structures due to the accumulation of spattered melt during WEDM. When the sample surface is cut for the second time, the number of craters on the aluminum alloy surface per unit area increases significantly due to the decrease of crater size, ranging from 20 to 60 μm (as shown in Fig. 3c). The increase of the number of craters also results in the increase of the number of porous structures around the craters, as shown in the Fig. 3d. After cutting the sample for the third time (as shown in Fig. 3e and f), the crater size continues to decrease (15–20 μm), while the number of crater and porous structure increases correspondingly. Following the forth cutting (as shown in Fig. 3g), the size of craters reached the minimum, ranging from 5 to 15 μm, displaying the largest number of craters. At the same time, the number of the porous structure increases significantly (as shown in Fig. 3h), which is very conducive to the storage of lubricating oil. Fig. 4 is the 3D morphology of the treated surface by WEDM with different cutting times. It can be observed that with the increase of cutting times, the size of surface crater decreases but the number increases, which also leads to the increase of the number of porous microstructure.

Fig. 5 shows the wetting state of water droplets on the SLIPS. As shown in Fig. 5a, the CA of water droplet on the SLIPS is 110.65 ± 1.14°, exhibiting excellent hydrophobicity. Sliding process of water droplet on the SLIPS was also investigated in this paper as shown in Fig. 5b1 and b2. The average sliding velocity of water droplet (10 μL) is 0.48 ± 0.05 mm s^{-1} at a sliding angle (SA) of 5°. In addition, the sliding state of the dyed acid droplet (pH = 3), alkali droplet (pH = 13), salt droplet (3.5% NaCl solution) and water droplet on the SLIPS are shown in Fig. 5c–f. It can be seen that the droplets can easily slide on the surface, although the surface tilt angle is very small, it still shows a smooth sliding. It indicates that the WEDM aluminum alloy surface can be injected lubricating oil to achieve superslippery property.

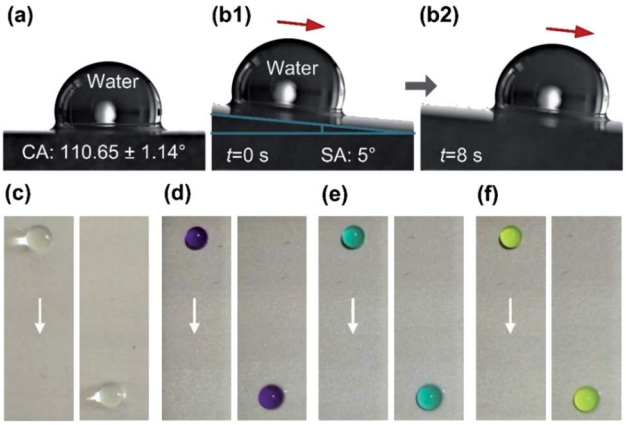

Fig. 5 Wetting state of water droplets on SLIPS. (a) CA of water droplet on SLIPS. (b1) and (b2) Sliding state of water droplet on SLIPS. (c–f) Motion results of different kinds of droplets on SLIPS inclined at an angle of 10 degrees: (c) acid droplet, PH = 3. (d) Alkali droplet, PH = 13. (e) Salt droplet, 3.5% NaCl solution. (f) Water droplet.

3.2. Corrosion current density, corrosion potential and impedance analysis

Fig. 6 illustrates the polarization curves of the PS, WEDMS, FWEDMS and SLIPS after immersion in 3.5 wt% NaCl solution. Table 2 shows the corrosion potential (E_{corr}), corrosion current (I_{corr}) and corrosion protection efficiency (IE) of the sample

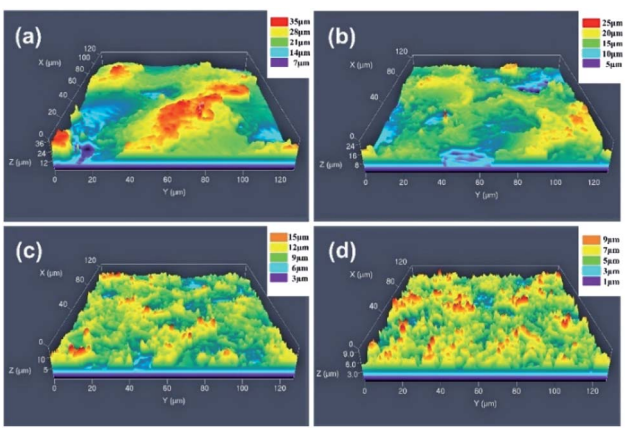

Fig. 4 3D morphology of treated surface by WEDM with different cutting times. (a) First cutting. (b) Second cutting. (c) Third cutting. (d) Fourth cutting.

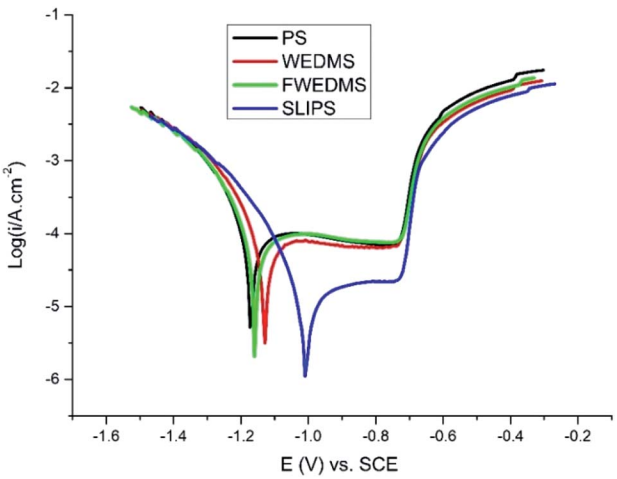

Fig. 6 Polarization curves of the PS, WEDMS, FWEDMS and SLIPS after immersion in 3.5 wt% NaCl solution.

Table 2 Corrosion potential (E_{corr}), corrosion current (I_{corr}) and corrosion protection efficiency (IE) of aluminum alloy sample surface with different treatment methods after immersion in 3.5 wt% NaCl solution

Samples	E_{corr} (V)	I_{corr} (A cm^{-2})	IE
PS	−1.1710	1.119×10^{-4}	—
WEDMS	−1.1304	7.175×10^{-5}	35.88%
FWEDMS	−1.1593	5.606×10^{-5}	49.90%
SLIPS	−1.0071	3.116×10^{-6}	97.22%

surface with different treatment methods. Compared to PS, the corrosion current density of the WEDMS decreases slightly from 1.119×10^{-4} A cm^{-2} to 7.175×10^{-5} A cm^{-2}. After modified by fluorosilane, the corrosion current density of the WEDMS further reduces to 5.606×10^{-5} A cm^{-2}. The SLIPS has the smallest corrosion current density of 3.116×10^{-6} A cm^{-2}, decreased by about two orders of magnitude compared with the PS. Additionally, the corrosion potential of the WEDMS, FWEDMS and SLIPS shifts to the right relative to the PS, and the offset of the SLIPS is the largest, increased by 0.1639 V.

The increase of corrosion potential and the decrease of corrosion current density indicate that the SLIPS effectively inhibits the anodic solubility of the aluminum alloy. This is similar to the results of Jeong[33] and Dong[34] discussed in reducing the corrosion current density by using electrochemical anodizing technique and sand peening method. The oil film formed by the injection of lubricating oil plays an important role in preventing the direct contact between the chloride ions and the surface of the sample, thereby improving the corrosion resistance of the aluminum alloy surface in a corrosive environment. The corrosion protection efficiency of aluminum alloy sample surface treated by different methods can be calculated by the corrosion current density of the surface. The equation is as follows:

$$\mathrm{IE} = \frac{I_0 - I}{I_0} \times 100\% \quad (1)$$

where, I_0 is the corrosion current density of the PS and I is the corrosion current density of the WEDMS, FWEDMS and SLIPS. According to the equation, the corrosion protection efficiency of WEDMS, FWEDMS and SLIPS is 35.88%, 49.90% and 97.22%, respectively, as shown in Table 2.

Fig. 7 presents the Nyquist plots of the PS, WEDMS, FWEDMS and SLIPS. The PS has an impedance radius of approximately 4 kΩ cm^2. Compared to the PS, the impedance of the WEDMS is increased, and the impedance radius is about 2 times higher than that of the PS. The reason is that the air filled in the porous microstructures of the WEDMS forms an air layer, which prevents corrosive chloride ions from coming into contact with the metal substrate. But this kind of air layer is unstable and will be destroyed under certain conditions, such as high liquid pressure. In the process of WEDM, as the cutting fluid is oil organic matter, a large amount of free carbon (the weight percentage of carbon element increases 14.9% by WEDM) is produced by decomposition at high temperature,

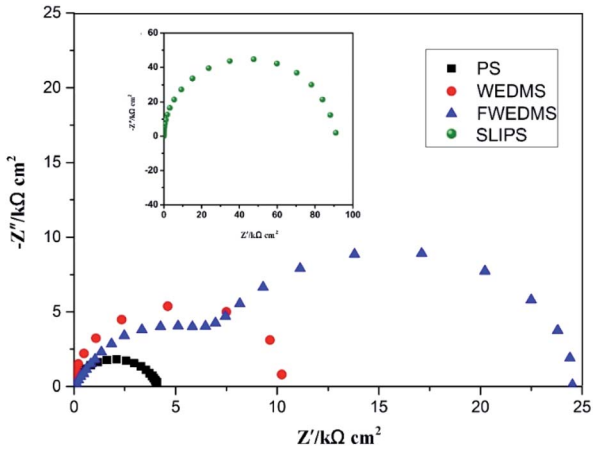

Fig. 7 Nyquist plots of aluminum alloy samples surface treated by different methods.

which is attached to the surface layer of substrate after cooling. So the carbon layer also plays an important role in the corrosion resistance of the material. In addition, the improvement of corrosion resistance of WEDMS compared to PS may be related to the forming microstructure due to the re-melting of the surface during the WEDM. For the FWEDMS, the impedance further increases, and the impedance radius reaches 25 kΩ cm^2. It can be explained that the hydrophobicity of the surface is enhanced after modification, approximating to super-hydrophobicity (CA is about 149°), and a more stable air layer is formed between the metal substrate and the corrosion solution. The impedance of the SLIPS is the largest, and the impedance radius reaches 90 kΩ cm^2, which is about 20 times than that of the PS. This high impedance characteristic is due to the fact that the liquid lubricanting oil completely covers the entire sample surface and the formation of stable oil film inhibits the electron transfer between the substrate and the corrosion solution.

3.3. Analysis of corrosion resistance based on salt solution immersion experiment

Fig. 8 is the optical image of aluminum alloy samples surface treated by different methods before and after immersion in

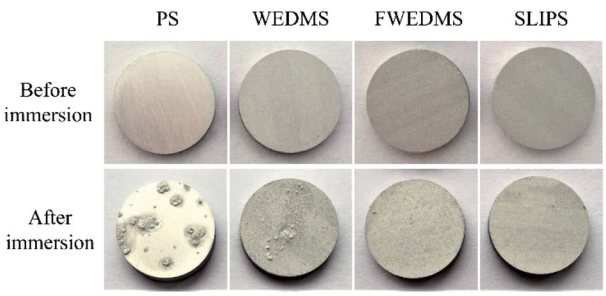

Fig. 8 Optical image of aluminum alloy samples surface treated by different methods before and after immersion in 3.5 wt% NaCl solution for 21 days. From left to right are PS, WEDMS, FWEDMS and SLIPS. The first line is the sample surface before immersion and the second line is the sample surface after immersion.

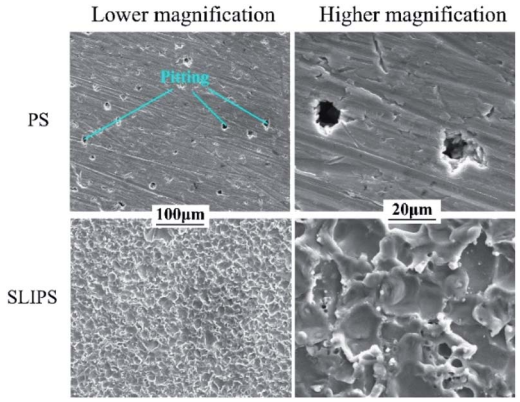

Fig. 9 SEM images of aluminum alloy surface treated by different methods after 21 days of immersion in 3.5 wt% NaCl solution. The first line are the SEM images of the PS at lower and higher magnification. The second line are the SEM images of the SLIPS at lower and higher magnification.

3.5 wt% NaCl solution for 21 days (from left to right are PS, WEDMS, FWEDMS and FLIPS). As shown in the first line, the PS, WEDMS and FWEDMS are initially smooth and clean, while the SLIPS is covered with an oil film before immersion. It can be observed that a layer of loose white substance appears on the PS after 21 days of immersion, which are salty contaminants and corrosion products deposited on the surface of aluminum alloy samples. We can see there are fewer loose white substance on the WEDMS than that of the PS, and the FWEDMS and SLIPS are as clean as before immersion. Salt solution immersion experiments show that both the FWEDMS and SLIPS provide strong corrosion resistance. This also confirms the previous results of potentiodynamic polarization curve measurement and electrochemical impedance spectroscopy test, SLIPS has stronger corrosion resistance.

Fig. 9 shows the SEM image of aluminum alloy surface treated by different methods after 21 days of immersion in 3.5 wt% NaCl solution. A large number of corrosion voids are observed on the PS, with a diameter of about 10 μm (Fig. 9, SEM images of the PS), that is, pitting of aluminum alloy. The minimum number of corrosion voids are found on the SLIPS (Fig. 9, SEM images of the SLIPS), and the results indicate that the SLIPS has good corrosion resistance in the corrosion environment of 3.5 wt% NaCl solution.

In order to further study the corrosion state of different surfaces in salt solution, the four groups of samples after immersion were taken out from the salt solution, and then cleaned in alcohol and deionized water by ultrasonic vibration in turn, the surface elements were observed using EDS after drying. Table 3 shows the changes of Al, O, F, Na and Cl elements on the PS, WEDMS, FWEDMS and SLIPS before and after immersion in 3.5 wt% NaCl solution for 21 days. It is found that the weight percentage of Al element on PS decreases from 98.9% to 92.1%, while O element increases from 1.1% to 5.2% after immersion. The corrosion of aluminum alloy makes Al^{3+} ions enter into the solution to reduce the weight percentage of Al element. Meanwhile, part of the generated Al^{3+} ions diffuse outside the pitting, usually forming an aluminum hydroxide layer which increases the weight percentage of O element on the sample surface (see Section 3.4 for details). Furthermore, Na and Cl elements on the surface are observed, indicating that corrosion occurred on the PS in NaCl solution. A small amount of Na and Cl elements are observed on the WEDMS and FWEDMS after 21 days of immersion in NaCl solution, and the weight percentage of O element increased compared with that before immersion (WEDMS: from 15.1% to 18.6%, FWEDMS: from 16.1% to 16.4%). The increase of weight percentage O element on FWEDMS is less than that on WEDMS. This means that the corrosion degree of the WEDMS is lower than that of the PS, and the corrosion degree of the FWEDMS is the lowest among them. For the SLIPS, Na and Cl elements are not detected on the surface after 21 days of immersion in NaCl solution, indicating that the surface exhibited strong corrosion resistance to the NaCl solution. On the other hand, F element is observed on the FWEDMS and SLIPS, with weight percentage of 1.1% and 1.2%, respectively. It is found that there is no significant change in the weight percentage of F element before and after immersion, indicating that the low surface energy film is not corroded in NaCl solution. It is further shown that the FWEDMS and SLIPS have good corrosion resistance stability in 3.5 wt% NaCl solution.

The wettability of SLIPS was tested to further study the corrosion resistance stability and durability of the SLIPS in the salt solution during the immersion process. Fig. 10 shows the wettability of SLIPS immersed in 3.5 wt% NaCl solution for different days. It can be seen that the CA of water droplets on the SLIPS without immersion is 110.35°. With the increase of immersion days, the CA has a downward trend. In the first three

Table 3 Changes of elements Al, O, F, Na and Cl on aluminum alloy surface treated by different methods before and after immersion in 3.5 wt% NaCl solution for 21 days

	Elemental composition and content (wt%)									
	Al		O		F		Na		Cl	
Sample types	Day 0	Day 21	Day 0	Day 21	Day 0	Day 21	Day 0	Day 21	Day 0	Day 21
PS	98.9	92.1	1.1	5.2	—	—	—	0.9	—	1.8
WEDMS	84.9	81.5	15.1	18.6	—	—	—	0.3	—	0.6
FWEDMS	82.7	82.6	16.1	16.4	1.2	1.1	—	0.3	—	0.5
SLIPS	82.7	82.7	16.1	16.1	1.2	1.2	—	—	—	—

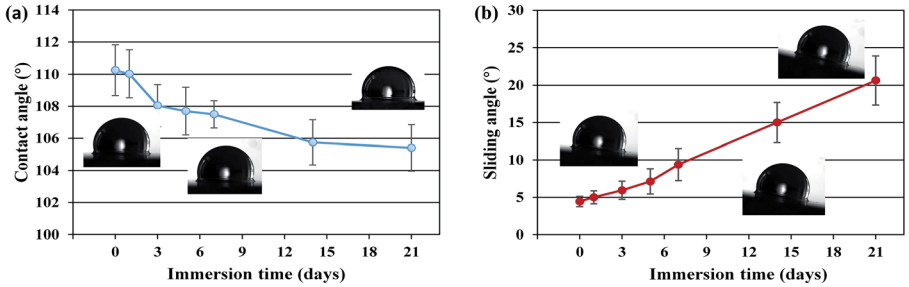

Fig. 10 The wettability of SLIPS immersed in 3.5 wt% NaCl solution for different days. (a) CA. (b) SA.

days of immersion, the CA decreases from 110.25° to 108.12°, demonstrating an obvious downward trend. This may be related to the desaturation of lubricating oil because excessive oil will saturate the porous surface. During the 3–21 days of immersion, the CA varied from 108.13–105.47° with a small change (Fig. 10a). However, the SA increases gradually with increasing immersion days. In Fig. 11b, it can be seen that the SA of water droplets on the surface without immersion is about 5°, after 21 days of immersion in NaCl solution, the SA increases to about 20°, but it still shows good hydrophobicity. The reason for the stable wettability of the SLIPS may be that the lubricating oil film becomes thinner but not completely destroyed during immersion in NaCl corrosion solution. Therefore, the SLIPS can achieve good corrosion resistance stability and durability in 3.5 wt% NaCl solution environment.

3.4. Surface corrosion characteristics and corrosion resistance mechanism

In fact, the surface of the aluminum alloy will undergo the following corrosion reaction in the NaCl solution. When the NaCl solution is in contact with the aluminum alloy substrate, the reaction formula is as follows:

$$Al + 3H_2O = Al(OH)_3 + \frac{3}{2}H_2 \quad (2)$$

Then, the boehmite produced in the previous step will be dissolved by chloride ions. The reaction formulas are as follows:

$$Al(OH)_3 + Cl^- = Al(OH)_2Cl + OH^- \quad (3)$$

$$Al(OH)_2Cl + Cl^- = Al(OH)Cl_2 + OH^- \quad (4)$$

$$Al(OH)Cl_2 + Cl^- = AlCl_3 + OH^- \quad (5)$$

Meanwhile, the direct contact between chloride ion and aluminum alloy substrate will aggravate the anodic dissolution of the substrate, resulting in pitting, as shown in formula (6). Part of the generated Al^{3+} ions diffuse outside the pitting, usually forming an aluminum hydroxide layer at the edge of the pitting, which hinders the further outward dispersion of Al^{3+} ions. The concentration of metal ions in corrosion voids is higher than that outside due to the aggregation of Al^{3+} ions, that is, excess positive charge. Therefore, the external chloride ions will continue to enter pitting to maintain charge balance. At the same time, the hydrolysis of Al^{3+} ions in pitting increases the acidity of the local solution, resulting in a decrease in the pH value, as shown in formula (7). The hydrolysis of chloride caused by the large amount of chloride ions will further aggravate the acidification of corrosion solution, thus promoting the continuation of corrosion.

$$Al = Al^{3+} + 3e^- \quad (6)$$

$$Al^{3+} + 3H_2O = Al(OH)_3 + 3H^+ \quad (7)$$

During immersion in 3.5 wt% NaCl solution, first, an air layer will be formed on the FWEDMS to prevent the corrosion liquid from wetting the surface (Fig. 11a). Second, for the hydrophobic surface of FWEDMS, it is negatively charged in neutral solutions. Among the negative ions, corrosive chloride ions has the lowest saturation coverage. The negative charging of a hydrophobic surface causes a redistribution of ions inside the double electric layer leading to the depletion of chloride anion concentration in the vicinity of a solid surface.[35] Finally, the well-ordered layer of a hydrophobic agent acts as a barrier for charge transfer, corrosive chloride ions cannot penetrate into the substrate, and the possibility of corrosion reaction on the FWEDMS is lower than that on the PS. For SLIPS, a barrier to isolate corrosion solution is formed on the surface due to the injection of high density and low surface energy lubricating oil, as shown in Fig. 11b. Moreover, the high strength porous microstructure produced by WEDM can lock the lubricant

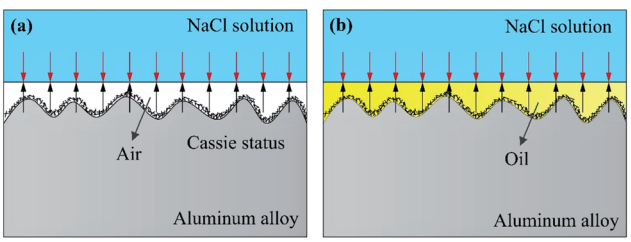

Fig. 11 The schematic diagram of corrosion resistance mechanism of solid–liquid two-phase contact interface between aluminum alloy surface and 3.5 wt% NaCl solution under different treatment conditions (a) FWEDMS, with air layer. (b) SLIPS, with oil layer.

firmly on the surface of the sample, which makes the barrier more stable and extremely difficult to penetrate by corrosion solution. In addition, lubricating oil with fluid properties spontaneously flow to the defective areas on the surface through capillary action driven by surface energy, resulting in self-healing ability, which significantly improves the surface defect induction and aggravation of corrosion problems. In conclusion, the SLIPS has better corrosion resistance in NaCl corrosion solution environment.

4. Conclusions

A novel WEDM technology was used to construct high strength porous microstructures on 7075 aluminum alloy surfaces. Perfluorinated lubricating oil was injected into the surface after fluorosilane treatment to obtain the SLIPS. Evaluated by potentiodynamic polarization curve measurement, electrochemical impedance spectroscopy test and immersion experiment in 3.5 wt% NaCl solution, SLIPS has been proved to have better stable and durable corrosion resistance than other three surfaces PS, WEDMS and FWEDMS. The corrosion current density of the SLIPS is 2 orders of magnitude lower than that of the polished surface. And the impedance radius is about 20 times than that of the polished surface. The results of wettability analysis show that the prepared SLIPS can achieve superslippery property, and the SA is less than 5°. Meanwhile, the self-healing ability of lubricating oil with fluid properties can significantly improve the surface defect induction and corrosion problems. Furthermore, the processing of planar and various complex shapes of cavity can be achieved, and WEDM has been proved to be effective in fabricating porous microstructure on metal substrates, which provides a new idea for fabricating porous microstructure with large area and low cost, and widens the potential application of the SLIPS.

Author contributions

Yu, P. drafted the manuscript and performed the experiments; Lian, Z. X. contributed to the design of the work; Xu, J. K. performed the interpretation of data; Yu, H. D. was responsible for substantive revision.

Conflicts of interest

We declare that we have no competing financial interest and personal relationships with other people or organizations that could inappropriately influence our work. There are no personal or corporate interests that could affect manuscript review.

Acknowledgements

This work was supported by the National Natural Science Foundation of China (No. U19A20103), National Key Research and Development Plan Project (No. 2018YFB1107403), the Jilin Province Scientific and Technological Development Program (No. Z20190101005JH), and the "111" Project of China (No. D17017).

References

1 G. L. Chen, M. H. Chen, N. Wang and J. W. Sun, Hot forming process with synchronous cooling for AA2024 aluminum alloy and its application, *Int. J. Adv. Des. Manuf. Technol.*, 2016, **86**, 133–139.
2 H. D. Yu, Z. X. Lian, Y. L. Wan, Z. K. Weng, J. K. Xu and Z. J. Yu, Fabrication of durable superamphiphobic aluminum alloy surfaces with anisotropic sliding by HS-WEDM and solution immersion processes, *Surf. Coat. Technol.*, 2015, **275**, 112–119.
3 R. J. Liao, Z. P. Zuo, C. Guo, Y. Yuan and A. Y. Zhuang, Fabrication of superhydrophobic surface on aluminum by continuous chemical etching and its anti-icing property, *Appl. Surf. Sci.*, 2014, **317**, 701–709.
4 S. A. Abdel-Gawad, M. A. Sadik and M. A. Shoeib, Preparation and properties of a novel nano Ni-B-Sn by electroless deposition on 7075-T6 aluminum alloy for aerospace application, *J. Alloys Compd.*, 2019, **785**, 1284–1292.
5 H. G. Wei, Y. R. Wang, J. Guo, N. Z. Shen, D. W. Jiang, X. Zhang, X. R. Yan, J. H. Zhu, Q. Wang, L. Shao, H. F. Lin, S. Y. Wei and Z. H. Guo, Advanced micro/nano capsules for self-healing smart anticorrosion coatings, *J. Mater. Chem. A*, 2015, **3**, 469–480.
6 R. Ly, K. T. Hartwig and H. Castaneda, Effects of strain localization on the corrosion behavior of ultra-fine grained aluminum alloy AA6061, *Corros. Sci.*, 2018, **139**, 47–57.
7 Y. J. Yang, J. H. Lee, I. C. Park and S. J. Kim, Investigation on Electrochemical Cathodic Protection for Cavitation-Erosion Reduction of Anodized Al Alloy, *J. Nanosci. Nanotechnol.*, 2020, **20**, 5658–5661.
8 W. T. Huo, X. Lin, S. Yu, Z. T. Yu, W. Zhang and Y. S. Zhang, Corrosion behavior and cytocompatibility of nanograined AZ31 Mg alloy, *J. Mater. Sci.*, 2019, **54**, 4409–4422.
9 Z. X. Lian, J. K. Xu, Z. B. Wang and H. D. Yu, Biomimetic superlyophobic metallic surfaces focusing on their fabrication and applications, *Journal of Bionic Engineering*, 2020, **17**, 1–33.
10 L. F. Yuan, T. Z. Wu, W. J. Zhang, S. Q. Ling, R. Xiang, X. C. Gui, Y. Zhu and Z. K. Tang, Engineering superlyophobic surfaces on curable materials based on facile and inexpensive microfabrication, *J. Mater. Chem. A*, 2014, **2**, 6952–6959.
11 J. L. Song, Z. A. Liu, X. Y. Wang, H. Liu and L. P. Parkin, High-Efficiency Bubbles Transportation in Aqueous Environment on Serial-Wedge-Shaped Wettability Pattern, *J. Mater. Chem. A*, 2019, **7**, 13567–13576.
12 J. Sun, W. Cheng, J. L. Song, Y. Lu, Y. K. Sun, L. Huang, X. Liu, Z. J. Jin, C. J. Carmalt and L. P. Parkin, Fabrication of Superhydrophobic Micro Post Array on Aluminum Substrates Using Mask Electrochemical Machining, *Chin. J. Mech. Eng.*, 2018, **31**, 1–7.
13 T. S. Wong, S. H. Kang, S. K. Y. Tang, E. J. Smythe, B. D. Hatton, A. Grinthal and J. Aizenberg, Bioinspired self-repairing slippery surfaces with pressure-stable omniphobicity, *Nature*, 2011, **477**, 443–447.

14 Z. X. Lian, J. K. Xu, Z. J. Yu, P. Yu and H. D. Yu, A simple two-step approach for the fabrication of bio-inspired superhydrophobic and anisotropic wetting surfaces having corrosion resistance, *J. Alloys Compd.*, 2019, **793**, 326–335.

15 Y. K. Wang, Y. P. Liu, J. Li, L. W. Chen, S. L. Huang and X. L. Tian, Fast self-healing superhydrophobic surfaces enabled by biomimetic wax regeneration, *Chem. Eng. J.*, 2020, **390**, 124311.

16 N. E. Sataeva, L. B. Boinovich, K. A. Emelyanenko, A. G. Domantovsky and A. M. Emelyanenko, Laser-assisted processing of aluminum alloy for the fabrication of superhydrophobic coatings withstanding multiple degradation factors, *Surf. Coat. Technol.*, 2020, **397**, 125993.

17 W. Li, X. H. Zhang, X. F. Yu, G. Wu, Y. Lei, G. Sun and B. You, Near infrared light responsive self-healing superhydrophobic coating based on solid wastes, *J. Colloid Interface Sci.*, 2020, **560**, 198–207.

18 J. Sun, C. Wang, J. L. Song, L. Huang, Y. K. Sun, Z. A. Liu, C. L. Zhao and Y. X. Li, Multi-functional application of oil-infused slippery Al surface: from anti-icing to corrosion resistance, *J. Mater. Sci.*, 2018, **53**, 16099–16109.

19 Z. P. Zuo, R. J. Liao, C. Guo, Y. Yuan, X. T. Zhao, A. Y. Zhuang and Y. Y. Zhang, Fabrication and anti-icing property of coral-like superhydrophobic aluminum surface, *Appl. Surf. Sci.*, 2015, **331**, 132–139.

20 S. S. Xu, Q. Wang, N. Wang and Z. Xu, Fabrication of superhydrophobic green surfaces with good self-cleaning, chemical stability and anti-corrosion properties, *J. Mater. Sci.*, 2019, **54**, 13006–13016.

21 A. K. Epstein, T. S. Wong, R. A. Belisle, E. M. Boggs and J. Aizenberg, Liquid-infused structured surfaces with exceptional anti-biofouling performance, *Proc. Natl. Acad. Sci. U. S. A.*, 2012, **109**, 13182–13187.

22 J. L. Song, L. Huang, C. L. Zhao, S. Wu and Y. W. Sun, Robust Superhydrophobic Conical Pillars from Syringe Needle Shape to Straight Conical Pillar Shape for Droplet Pancake Bouncing, *ACS Appl. Mater. Interfaces*, 2019, **11**, 45345–45353.

23 L. B. Boinovich, A. M. Emelyanenko, A. D. Modestov, A. G. Domantovsky, A. A. Shiryaev, K. A. Emelyanenko, O. V. Dvoretskaya and A. A. Ganne, Corrosion behavior of superhydrophobic aluminum alloy in concentrated potassium halide solutions: When the specific anion effect is manifested, *Corros. Sci.*, 2016, **112**, 517–527.

24 Y. Q. Wang, Y. Shi, L. J. Pan and M. Yang, Multifunctional superhydrophobic surfaces templated from innately microstructured hydrogel matrix, *Nano Lett.*, 2014, **14**, 4803–4809.

25 D. T. Ge, L. L. Yang, Y. F. Zhang, Y. D. Rahmawan and S. Yang, Transparent and superamphiphobic surfaces from one-step spray coating of stringed silica nanoparticle/sol solutions, *Part. Part. Syst. Charact.*, 2014, **31**, 763–770.

26 X. L. Wang, H. Y. Hu, Q. Ye and T. T. Gao, Superamphiphobic coatings with coralline-like structure enabled by one-step spray of polyurethane/carbon nanotube composites, *J. Mater. Chem.*, 2012, **22**, 9624–9631.

27 J. Zhang, R. Marega, L. J. Chen, N. W. Wu, X. D. Xu, D. C. Muddiman, D. Bonifazi and H. B. Yang, Hierarchical self-assembly of supramolecular hydrophobic metallacycles into ordered nanostructures, *Chem.–Asian J.*, 2014, **9**, 2928–2936.

28 L. Passoni, G. Bonvini, A. Luzio, A. Facibeni, C. E. Botani and F. Di Fonzo, Multiscale effect of hierarchical self-assembled nanostructures on superhydrophobic surface, *Langmuir*, 2014, **30**, 13581–13587.

29 P. Kim, T. S. Wong, J. Alvarenga, M. J. Kreder, W. E. Adorno-Martinez and J. Aizenberg, Liquid-infused nanostructured surfaces with extreme anti-Ice and anti-frost performance, *ACS Nano*, 2012, **6**, 6569–6577.

30 Y. H. Yeong, C. Y. Wang, K. J. Wynne and M. Gupta, Oil-infused superhydrophobic silicone material for low ice adhesion with long term infusion stability, *ACS Appl. Mater. Interfaces*, 2016, **8**, 32050–32059.

31 Y. L. Wan, L. N. Xu, Z. G. Liu and H. D. Yu, Fabrication of a super-amphiphobic aluminium alloy surface via wire electrical discharge machining and chemical etching technology, *Micro Nano Lett.*, 2017, **12**, 175–178.

32 J. K. Xu, R. X. Qiu, Z. X. Lian, Z. J. Yu, P. Yu, W. F. Ren and H. D. Yu, Wear and corrosion resistance of electroforming layer after WEDM for 7075 aluminum alloy, *Mater. Res. Express*, 2018, **5**, 066502.

33 C. Y. Jeong and J. H. Jeong, Fabrication of Superhydrophobic Aluminum Alloy Surface with Hierarchical Pore Nanostructure for Anti-Corrosion, *Corros. Sci. Technol.*, 2019, **18**, 228–231.

34 X. J. Dong, J. B. Meng, Y. Z. Hu, X. T. Wei, X. S. Luan and H. A. Zhou, Fabrication of Self-Cleaning Superhydrophobic Surfaces with Improved Corrosion Resistance on 6061 Aluminum Alloys, *Micromachines*, 2020, 11.

35 L. B. Boinovich, A. M. Emelyanenko, A. D. Modestov, A. G. Domantovsky and K. A. Emelyanenko, Not simply repel water: the diversified nature of corrosion protection by superhydrophobic coatings, *Mendeleev Commun.*, 2017, **27**, 254–256.